while the distance reflected in a one-dimensional finite difference approximation is limited by the criterion $hL/k \lesssim 1/20$ [3]. Since the present results allow $B_i = 4$ at least, $d_{ave}/L \approx 50$ or more. Because the time spent computing the distance from the position of a walker to the nearest boundary of a domain is the most time consuming part of a Monte Carlo procedure [4–6] this increase in average step size is significant since fewer steps would be required to complete a walk.

A less accurate single formulation for all included angles is available [8], obtained through application of the heat balance integral method, with less than about 1% error for $B_i < 1$.

*Acknowledgement*—The partial support of the National Science Foundation under Grant No. ENG77-27614 is acknowledged.

## REFERENCES

1. A. Haji-Sheikh and E. M. Sparrow, The solution of heat conduction problems by probability methods, *Trans. Am. Soc. Mech. Engrs, J. Heat Transfer* **89**, 121–131 (1967).
2. M. N. Rao, Solutions to heat-conduction problems by a mixed method, *Int. J. Heat Mass Transfer* **23**, 443–450 (1982).
3. A. Haji-Sheikh, Application of Monte Carlo methods to thermal conduction problems, Ph.D. Thesis, University of Minnesota, Minneapolis, p. 123 (1965).
4. T. J. Hoffman and N. E. Banks, Monte Carlo surface density solution to the Dirichlet heat transfer problem, *Nucl. Sci. Engng* **59**, 205–214 (1976).
5. J. H. Turner, An improved Monte Carlo procedure for the solution of the steady-state, two-dimensional diffusion equation with application to flow through porous media, M.S. Thesis, University of Kansas, Lawrence (1978).
6. J. H. Turner, Improved Monte Carlo procedures for the unsteady diffusion equation applied to water well fields, Ph.D. Thesis, University of Kansas, Lawrence (1982).
7. M. Ahmadian, J. H. Turner, and L. C. Burmeister, A Monte Carlo procedure for two-dimensional steady conduction at straight convecting boundaries, *ASME Paper*, No. 80-WA/HT-42, Am. Soc. Mech. Engrs, New York.

*Int. J. Heat Mass Transfer.* Vol. 28, No. 3, pp. 720–723, 1985
Printed in Great Britain

0017-9310/85 $3.00 + 0.00


# A numerical study of natural convection in a vertical, annular, porous layer

C. E. HICKOX and D. K. GARTLING
Fluid and Thermal Sciences Department, Sandia National Laboratories, Albuquerque, NM 87185, U.S.A.

(*Received* 17 *January* 1984 *and in revised form* 5 *July* 1984)

## 1. INTRODUCTION

IN THIS note, we summarize the results of a numerical study of natural convection in an annular porous layer. This work was undertaken in an effort to gain insight into the heat loss mechanisms associated with large insulated tanks. The original presentation of this work, as a conference paper [1], preceeded the publication of more comprehensive studies of the same geometry by Havstad and Burns [2] and Prasad and Kulacki [3]. Prior to the appearance of these papers, analyses were available only for planar porous layers, for which refs [4–7] are representative. Given the recent interest shown in annular porous layers, it seems appropriate to consider briefly the main results of ref. [1]. A numerical method was used in this work that is different from the methods used in either of the other two studies cited. In addition, the effects of anisotropic permeability are given brief consideration. The present work is thus complementary to refs [2 and 3].

## 2. THE VERTICAL, ANNULAR, POROUS LAYER

The two-dimensional, axisymmetric configuration which is to be studied is illustrated in Fig. 1. The height of the layer is denoted by $H$, the thickness by $W$, and the inner and outer radii by $R_i$ and $R_0$, respectively. All boundaries of the annular region are impermeable. Both horizontal boundaries are adiabatic and the vertical boundaries are maintained at constant temperatures $T_i$ and $T_0$ where it is assumed that $T_i > T_0$. The annular region is filled with a rigid, fluid-saturated, porous medium. Gravity acts in the negative $z$-direction. In general, the permeability in the radial direction can differ from that associated with the vertical direction.

It is convenient to normalize all lengths with respect to the inner radius $R_i$. The annular region can then be represented by an equivalent annular region with an inner radius of unity, a height of $H/R_i$, and a thickness of $W/R_i$, where $W = R_0 - R_i$. Then, the annular region can be defined by specifying the layer aspect ratio $H/W$ and the nondimensional height $H/R_i$. These latter two parameters are utilized in the presentation of the numerical results.

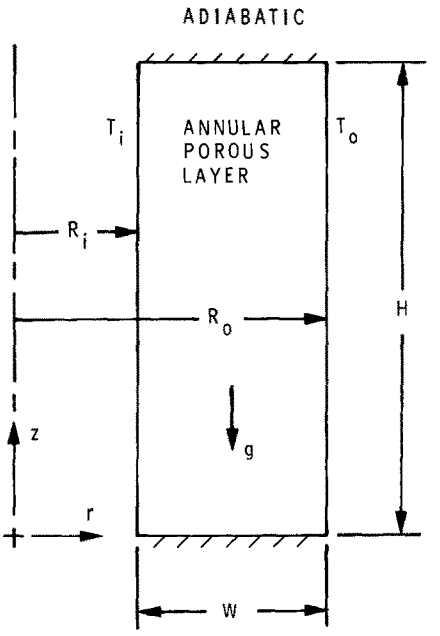


FIG. 1. The vertical, annular, porous layer.

## 3. MATHEMATICAL FORMULATION

The porous matrix is assumed to be rigid and the fluid incompressible with density changes occurring only as a result of changes in the temperature according to

$$\rho = \rho_0[1-\beta(T-T_0)] \tag{1}$$

where $\rho$ is the fluid density, $T$ is the temperature, $\beta$ is the coefficient of thermal expansion, and the subscripts refer to reference conditions. In accordance with the Boussinesq approximation, the effects of fluid density changes are accounted for in the buoyancy term in the equations of motion and are neglected elsewhere. All other fluid and solid properties are assumed constant. It is also assumed that the fluid and matrix are in thermal equilibrium and that the fluid motion can be adequately described by Darcy's law. The equations of continuity, motion, and thermal transport can then be expressed, respectively, as

$$\frac{1}{r}\frac{\partial}{\partial r}(ru)+\frac{\partial w}{\partial z}=0 \tag{2}$$

$$\frac{\mu}{k_{rr}}u=-\frac{\partial P}{\partial r},\quad \frac{\mu}{k_{zz}}w=-\frac{\partial P}{\partial z}+\rho_0 g\beta(T-T_0) \tag{3}$$

$$\rho_0 c\left(u\frac{\partial T}{\partial r}+w\frac{\partial T}{\partial z}\right)=\kappa_e\left(\frac{\partial^2 T}{\partial r^2}+\frac{1}{r}\frac{\partial T}{\partial r}+\frac{\partial^2 T}{\partial z^2}\right) \tag{4}$$

where the radial coordinate direction is denoted by $r$ and the vertical direction by $z$. The pressure term $P$ represents the quantity $(\bar{P}+\rho_0 gz)$ where $\bar{P}$ is the pore volume averaged pressure. The bulk volume averaged Darcy velocity components associated with the $(r, z)$ coordinates are denoted by $(u, w)$. The symbols $\kappa_e$, $c$, $\mu$, and $g$ are, respectively, effective thermal conductivity, fluid specific heat, viscosity, and acceleration of gravity. The intrinsic permeabilities in the radial and vertical directions are given by $k_{rr}$ and $k_{zz}$, respectively. Although the large majority of numerical results are for the isotropic case, $k_{rr}=k_{zz}$, the effects of anisotropy are evaluated for one specific geometry.

Rather than solving equations (2)–(4) directly, the numerical method to be considered subsequently utilizes the scalar equation for pressure

$$\frac{k_{rr}}{k_{zz}}\frac{1}{r}\frac{\partial}{\partial r}\left(r\frac{\partial P}{\partial r}\right)+\frac{\partial^2 P}{\partial z^2}=\rho_0 g\beta\frac{\partial T}{\partial z} \tag{5}$$

obtained by combining equations (2) and (3). Elimination of the velocity components from equation (4) through use of equations (3) provides an equation which can be solved simultaneously with equation (5) for the pressure $P$ and temperature $T$. Darcy's law, as given by equations (3), can then be used to obtain the velocity field.

In order to complete the mathematical description, appropriate boundary conditions must be specified for the specific problem under consideration. Since all boundaries of the porous layer are impermeable, the velocity component normal to a boundary must vanish on the boundary. The horizontal boundaries are insulated; hence, the condition of zero heat flux normal to the boundary is imposed. Finally, the temperatures on the inner and outer boundaries are specified by $T_i$ and $T_0$, as indicated in Fig. 1.

Equations (2)–(4) can be rendered nondimensional in such a way that the only new parameters which result, other than the geometrical ones already discussed, are the ratio of permeabilities $(k_{rr}/k_{zz})$ and the Rayleigh number

$$Ra=\frac{\rho_0^2 c g\beta k_{zz}W(T_i-T_0)}{\mu\kappa_e}. \tag{6}$$

This particular nondimensionalization is accomplished by selection of $R_i$ as a reference length, $(\kappa_e/\rho_0 cR_i)$ as a reference velocity, and $(\mu\kappa_e/\rho_0 ck_{zz})$ as a reference pressure. A suitable nondimensional temperature is given by $(T-T_0)/(T_i-T_0)$. The total nondimensional heat transfer rate across the annular layer can be expressed in terms of the Nusselt number

$$Nu=\frac{Q}{2\pi\kappa_e H(T_i-T_0)/\ln(R_0/R_i)} \tag{7}$$

where $Q$ is the total heat transfer rate and the denominator is the rate at which heat is conducted across the layer. We thus anticipate the following functional relationship among the various nondimensional parameters:

$$Nu=f(Ra, k_{rr}/k_{zz}, H/W, H/R_i). \tag{8}$$

It is this relationship which is investigated numerically.

## 4. COMPUTATIONAL APPROACH

Numerical solutions to equations (3)–(5) were obtained through use of a finite element computer program [8, 9] based on the Galerkin form of the finite element method. In the present study, we have considered only steady, axisymmetric, natural convection. Hence, our discussion will be limited to a brief description of the specific numerical approach utilized for the solution of the problem at hand.

Implementation of the finite element method is accomplished by first dividing the region of interest into a number of simply shaped subregions, or finite elements. Then, within each element, a set of nodal points is established at which the dependent variables $u$, $w$, $P$, and $T$ are evaluated. The dependent variables are represented within an element by suitably chosen approximating (basis) functions. In the particular method utilized in the present study, the pressure and temperature are approximated using quadratic basis functions and the velocity components are taken to be linear within each element. Application of the method of weighted

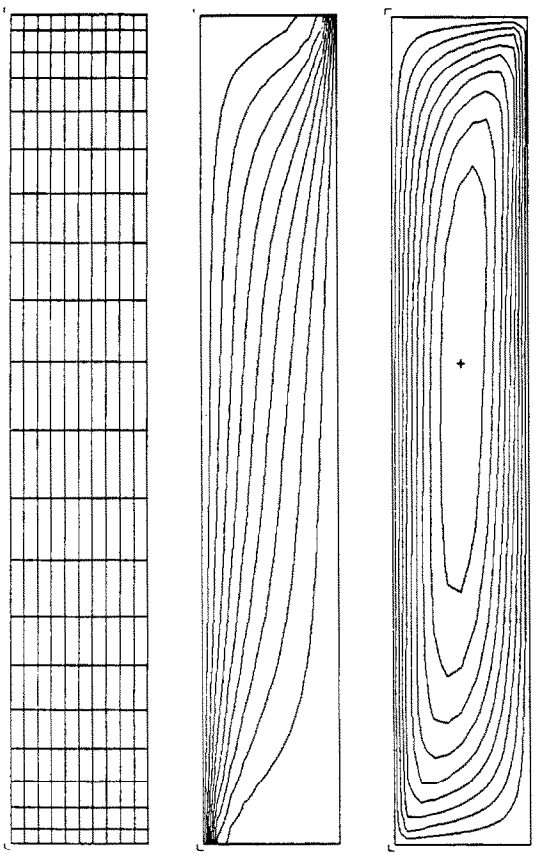

FIG. 2. Finite element grid and representative isotherms and streamlines for $Ra = 100$, $H/W = 6$, and $H/R_i = 4$.

residuals then results in a system of coupled, nonlinear, algebraic equations for the nodal point unknowns $u$, $w$, $P$, and $T$. A numerical procedure based on Picard iteration was used to obtain converged solutions for the steady-state problem. The solution of the system of algebraic equations was accomplished by a frontal elimination procedure which is a special variant of Gaussian elimination. The solution was assumed to have been adequately converged when the maximum difference between successive iterates of the temperature divided by the local temperature was less than the prescribed tolerance of $10^{-5}$ for all nodal points. For this convergence tolerance, the average Nusselt numbers computed for the inner and outer walls differed by less than 0.01%.

For purposes of analysis, the annular layer was discretized using a $10 \times 20$ mesh of eight-node, quadrilateral elements, with the thickness divided into ten equally spaced increments. The element spacing was graded in the vertical direction in order to provide increased resolution in regions where large spatial gradients of the dependent variables exist. A representative finite element grid is illustrated in Fig. 2.

Based on studies which we have reported previously in relation to planar geometries [7], it is anticipated that the number of elements used in the analysis is significantly larger than that required for acceptable accuracy. Furthermore, a recent study, reported by Reda [10], has shown excellent agreement between experimental results and predictions based on the computer program described in refs. [8 and 9].

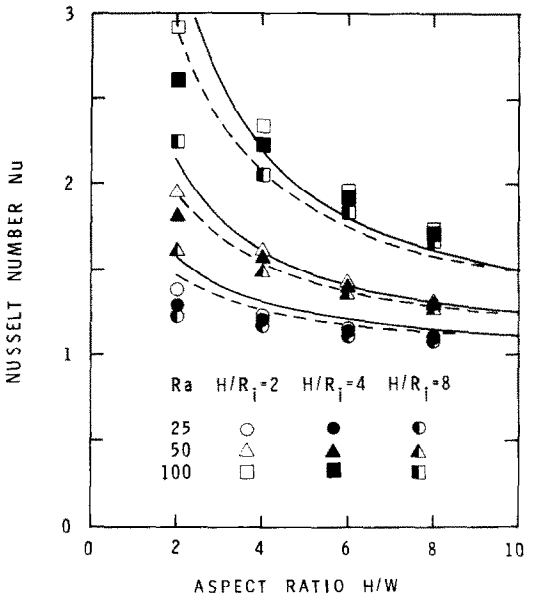


FIG. 3. Numerically predicted values for the Nusselt number. Solid and dashed curves are predictions from equation (9) for $H/R_i = 2$ (solid) and 8 (dashed).

## 5. NUMERICAL RESULTS

### 5.1. *Heat transfer rate*

Numerically determined values for the total heat transfer rate across the annular layer are tabulated in Table 1 for the case of isotropic permeability, with Rayleigh numbers in the range 25–100 and aspect ratios and ratios of layer height-to-inner radius ranging from 2 to 8. This information is also presented graphically in Fig. 3. Prasad and Kulacki [3] have compared our results with those obtained in their studies. For a Rayleigh number of 100 and aspect ratios of 2, 4, 6, and 8, they found a maximum difference of 4.8% between the two sets of computed Nusselt numbers. Since the results of Prasad and Kulacki [3] also compared favorably with those of Havstad and Burns [2], we conclude that our results are consistent with those previously published.

The ranges of parameters chosen for study were selected on the basis of their correspondence to systems of practical importance. The numerical results for these cases were obtained in relatively few iterations and at modest computational cost. Solutions at higher Rayleigh numbers are also possible though the computational expense is somewhat higher due to an increase in the number of iterations required for convergence. The first-order iterative method presently employed in the computer program imposes a practical limit on the convergence of steady-state flows. For the present problem, satisfactory convergence cannot be easily attained for Rayleigh numbers greater than 300 when the aspect ratio is unity.

In Table 2, the results of a preliminary study of the effects of anisotropic permeability are presented. In ref. [4] it is indicated that the effective permeability of fibrous insulating materials may vary by a factor of two depending on the flow direction relative to the fibers which make up the insulation. Hence, the results of Table 2 were computed assuming a permeability ratio $k_{rr}/k_{zz}$ of 0.5 for an aspect ratio of 6 and a height-to-inner radius ratio of 4. The total heat transfer rate was reduced over that computed for the case of isotropic permeability. Although the maximum reduction in heat transfer rate was only 2.5%, reductions of this magnitude can be significant in certain applications of thermal energy storage.

### 5.2. *Thermal and flow fields*

Plots of representative isotherms and streamlines, as calculated for an aspect ratio of 6 and a height-to-inner radius ratio of 4, are presented in Fig. 2 for a Rayleigh number of 100 and isotropic permeability. The isotherms are equally spaced between nondimensional values of 1 and 0 at the inner and outer surfaces, respectively, where the nondimensional temperature is given by $(T - T_0)/(T_i - T_0)$. The streamlines are equally spaced between a value of zero for the nondimensional stream function on the boundary of the layer and a maximum value of 15.084, where the stream function is rendered nondimensional by division by the quantity $(\kappa_e R_i/\rho_0 c)$. The location of the maximum value for the stream function is indicated by the small cross on the figure.

Table 1. Numerical results for Nusselt number as a function of Rayleigh number $Ra$, aspect ratio $H/W$, and height-to-inner radius ratio $H/R_i$

| | $Ra$ | | | | | | | | |
|---|---|---|---|---|---|---|---|---|---|
| | $H/R_i = 2$ | | | $H/R_i = 4$ | | | $H/R_i = 8$ | | |
| $H/W$ | 25 | 50 | 100 | 25 | 50 | 100 | 25 | 50 | 100 |
| 2 | 1.379 | 1.951 | 2.904 | 1.323 | 1.811 | 2.613 | 1.237 | 1.621 | 2.249 |
| 4 | 1.230 | 1.619 | 2.335 | 1.214 | 1.572 | 2.229 | 1.181 | 1.492 | 2.060 |
| 6 | 1.157 | 1.427 | 1.965 | 1.150 | 1.408 | 1.920 | 1.135 | 1.370 | 1.834 |
| 8 | 1.118 | 1.323 | 1.741 | 1.115 | 1.313 | 1.717 | 1.107 | 1.292 | 1.670 |

Table 2. Numerical results for Nusselt number $Nu'$ for anisotropic permeability ($k_{rr}/k_{zz} = 0.5$) as a function of Rayleigh number $Ra$ for $H/W = 6$ and $H/R_i = 4$. The Nusselt number $Nu$ for isotropic permeability is included for comparison

| $Ra$ | $Nu'$ | $Nu$ |
|---|---|---|
| 25 | 1.128 | 1.150 |
| 50 | 1.372 | 1.408 |
| 100 | 1.878 | 1.920 |

5.3. *Approximate solution for large aspect ratio*

An approximate analysis, for large aspect ratio, can be developed by following the approach of Burns, Chow and Tien [7] who, in turn, utilized reasoning originally proposed by Batchelor [11] in his studies of natural convection in closed cavities. A similar approach was also utilized by Havstad and Burns [2].

Although for brevity we omit the details of the analysis, it can be shown that the Nusselt number can be approximated by

$$Nu = 1 + \gamma Ra F(m)/(H/R_i), \tag{9}$$

where

$$F(m) = \frac{\ln m}{m-1}\left[\frac{m^2}{2} - \frac{m^4}{2(m^2-1)} + \frac{m^2-1}{8(\ln m)^2}\right] \tag{10}$$

and $m$ is the ratio $(R_0/R_i)$. This result differs in form from that of Havstad and Burns [2] owing to the definitions used for the Nusselt and Rayleigh numbers. Based on the assumptions inherent in the analysis, it is anticipated that the approximate solution will be most valid for large aspect ratios and small Rayleigh numbers. In general, the factor $\gamma$ is a function of all the parameters identified in equation (8). Equation (9) is, however, most useful if $\gamma$ can be replaced with a suitably selected constant. For comparative purposes, the values of $\gamma$ predicted from the numerical results of Table 1 for an aspect ratio of 8 were averaged to yield a value of 0.585. Using this value, the Nusselt numbers predicted by equation (9) are plotted in Fig. 3. In ref. [2] a value of 0.57 is quoted for $\gamma$, which differs by only 3% from our result.

It is seen that the approximate results compare favorably with the numerical predictions for large aspect ratios and small Rayleigh numbers. An effect of curvature is apparent in the dependence of Nusselt number on the height-to-inner radius ratio $H/R_i$. This parameter is related to the radius ratio $m$ (as used by Prasad and Kulacki [3]) by $H/R_i = (H/W)(m-1)$. The agreement with the asymptotic theory is seen to improve as the radius ratio approaches unity, in agreement with the observations of Havstad and Burns [2] and Prasad and Kulacki [3].

## 6. CONCLUDING REMARKS

We have used a computer program based on the Galerkin form of the finite element method to perform a numerical study of steady, natural convection in a vertical, annular, porous layer. It was assumed that a constant temperature difference was maintained between the lateral surfaces of the layer. Numerical predictions of the heat transfer rate were obtained for Rayleigh numbers in the range 25–100 with aspect ratios and height-to-inner radius ratios ranging from 2 to 8. The range of parameters investigated was chosen to be typical of those associated with insulated tanks of the type used for thermal energy storage systems. Plots of representative isotherms and streamlines were presented for a typical geometry. The effects of anisotropic permeability were investigated in a preliminary manner.

For the range of parameters studied, the results indicated that the presence of natural convection in the annular layer could increase the heat transfer rate by a factor of as much as 2.6 times that due to thermal conduction. The preliminary study of the effects of nonisotropic permeability suggests that the overall heat transfer rate could be reduced by 2 to 3% provided the fibrous insulation is properly oriented. This latter result was obtained for an aspect ratio of 6 and a height-to-inner radius ratio of 4 for Rayleigh numbers ranging from 25 to 100. In general, the effects of anisotropic permeability will depend on the specific values chosen for the parameters involved.

*Acknowledgement*—The work described in this paper was performed at Sandia National Laboratories and was supported by the U.S. Department of Energy under Contract No. DE-AC04-76DP00789.

## REFERENCES

1. C. E. Hickox and D. K. Gartling, A numerical study of natural convection in a vertical, annular, porous layer, ASME Paper No. 82-HT-68, AIAA/ASME Third Joint Thermophysics, Fluids, Plasma, and Heat Transfer Conference, St. Louis, MO, June 7–11 (1982).
2. M. A. Havstad and P. J. Burns, Convective heat transfer in vertical cylindrical annuli filled with a porous medium, *Int. J. Heat Mass Transfer* **25**(11), 1755–1766 (1982).
3. V. Prasad and F. A. Kulacki, Natural convection in a vertical porous annulus, *Int. J. Heat Mass Transfer* **27**(2), 207–219 (1984).
4. P. J. Burns, L. C. Chow and C. L. Tien, Convection in a vertical slot filled with porous insulation, *Int. J. Heat Mass Transfer* **20**, 919–926 (1977).
5. C. G. Bankvall, Natural convection in vertical permeable space, *Warme-und Stoffubertragung* **7**, 22–30 (1974).
6. A. Bejan and C. L. Tien, Natural convection in a horizontal porous medium subjected to an end-to-end temperature difference, *J. Heat Transfer* **100**, 191–198 (1978).
7. C. E. Hickox and D. K. Gartling, A numerical study of natural convection in a horizontal porous layer subjected to an end-to-end temperature difference, *J. Heat Transfer* **103**, 797–802 (1981).
8. D. K. Gartling and C. E. Hickox, MARIAH—a finite element computer program for incompressible porous flow problems: theoretical background, SAND79-1622, Sandia National Laboratories, Albuquerque, NM (1982).
9. D. K. Gartling and C. E. Hickox, MARIAH—a finite element computer program for incompressible porous flow problems: user's manual, SAND79-1623, Sandia National Laboratories, Albuquerque, NM (1980).
10. D. C. Reda, Natural convection experiments in a liquid-saturated porous medium bounded by vertical coaxial cylinders, *J. Heat Transfer* **105**, 795–802 (1983).
11. G. K. Batchelor, Heat transfer by free convection across a closed cavity between vertical boundaries at different temperature, *Q. J. Appl. Math.* **12**, 209 (1954).